NeuroImage 64 (2013) 32–42

Contents lists available at SciVerse ScienceDirect

NeuroImage

journal homepage: www.elsevier.com/locate/ynimg

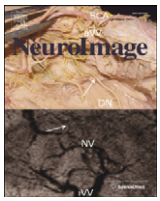

Predicting the location of human perirhinal cortex, Brodmann's area 35, from MRI

Jean C. Augustinack [a,*], Kristen E. Huber [a], Allison A. Stevens [a], Michelle Roy [a], Matthew P. Frosch [b], André J.W. van der Kouwe [a], Lawrence L. Wald [a], Koen Van Leemput [a,f], Ann C. McKee [c], Bruce Fischl [a,d,e] and For the Alzheimer's Disease Neuroimaging Initiative [1]

[a] Athinoula A Martinos Center, Dept. of Radiology, MGH, 149 13th Street, Charlestown MA 02129 USA
[b] C.S. Kubik Laboratory for Neuropathology, Pathology Service, MGH, 55 Fruit St., Boston MA 02115 USA
[c] Department of Pathology, Boston University School of Medicine, Bedford Veterans Administration Medical Center, MA 01730 USA
[d] MIT Computer Science and AI Lab, Cambridge MA 02139 USA
[e] MIT Division of Health Sciences and Technology, Cambridge MA 02139 USA
[f] Department of Informatics and Mathematical Modeling, Technical University of Denmark, Copenhagen, Denmark

ARTICLE INFO

Article history:
Accepted 21 August 2012
Available online 30 August 2012

Keywords:
Morphometry
Mesocortex
Alzheimer's disease
Localization

ABSTRACT

The perirhinal cortex (Brodmann's area 35) is a multimodal area that is important for normal memory function. Specifically, perirhinal cortex is involved in the detection of novel objects and manifests neurofibrillary tangles in Alzheimer's disease very early in disease progression. We scanned ex vivo brain hemispheres at standard resolution (1 mm × 1 mm × 1 mm) to construct pial/white matter surfaces in FreeSurfer and scanned again at high resolution (120 μm × 120 μm × 120 μm) to determine cortical architectural boundaries. After labeling perirhinal area 35 in the high resolution images, we mapped the high resolution labels to the surface models to localize area 35 in fourteen cases. We validated the area boundaries determined using histological Nissl staining. To test the accuracy of the probabilistic mapping, we measured the Hausdorff distance between the predicted and true labels and found that the median Hausdorff distance was 4.0 mm for the left hemispheres (n = 7) and 3.2 mm for the right hemispheres (n = 7) across subjects. To show the utility of perirhinal localization, we mapped our labels to a subset of the Alzheimer's Disease Neuroimaging Initiative dataset and found decreased cortical thickness measures in mild cognitive impairment and Alzheimer's disease compared to controls in the predicted perirhinal area 35. Our ex vivo probabilistic mapping of the perirhinal cortex provides histologically validated, automated and accurate labeling of architectonic regions in the medial temporal lobe, and facilitates the analysis of atrophic changes in a large dataset for earlier detection and diagnosis.

Introduction

The perirhinal cortex (Brodmann's area 35) is a multimodal cortical area that is located in the medial temporal lobe (MTL). A multimodal area receives input from more than one cortical association area and it is a region where information from different modalities converge (Jones and Powell, 1970; Van Hoesen and Pandya, 1975a). Perirhinal cortex is situated between the entorhinal cortex (Brodmann's area 28 and perirhinal's medial neighbor) and ectorhinal cortex (Brodmann's area 36 and perirhinal's lateral neighbor) in the mediolateral plane. The ectorhinal cortex (area 36) constitutes the perirhinal's anterior and lateral neighbor while the posterior parahippocampal cortex lies posterior to the perirhinal cortex.

Brodmann described the perirhinal cortex as a "transition between archipallium and neopallium" (Brodmann, 1909; Brodmann and Garey, 1994). Since then, the perirhinal cortex has undergone several name modifications. Braak and Braak coined the term 'transentorhinal' and succinctly described the mediolateral boundaries, but this description lacked the anterior-posterior entirety of the area (Braak and Braak, 1985). Perirhinal area 35 and transentorhinal are somewhat synonymous terms. To further complicate the situation for area 35, several investigators have lumped area 35 (perirhinal) and area 36 (ectorhinal) together and referred to it as perirhinal cortex (Suzuki and Amaral, 1994a,b), dropping the ectorhinal designation entirely and creating a very large area. Nonetheless, extensive rostrocaudal analyses with several histological stains have yielded the boundaries of the perirhinal cortex in the human brain, albeit including isocortical area 36 in the definition (Ding and Van Hoesen, 2010). To make matters even more confusing,

* Corresponding author at: Athinoula A Martinos Center, Massachusetts Gen. Hosp./ Harvard Med. School, Bldg. 149, 13th St., Charlestown, MA 02129, USA. Fax: +1 617 726 7422.
E-mail address: jean@nmr.mgh.harvard.edu (J.C. Augustinack).

[1] Data used in preparation of this article were obtained from the Alzheimer's Disease Neuroimaging Initiative (ADNI) database (adni.loni.ucla.edu). As such, the investigators within the ADNI contributed to the design and implementation of ADNI and/or provided data but did not participate in the analysis or writing of this report. A complete listing of ADNI investigators can be found at: http://adni.loni.ucla.edu/wp-content/uploads/how_to_apply/ADNI_Acknowledgement_List.pdf.

1053-8119/$ – see front matter © 2012 Elsevier Inc. All rights reserved.
http://dx.doi.org/10.1016/j.neuroimage.2012.08.071

perirhinal (area 35) and entorhinal (area 28) have also been grouped together and referred to as the rhinal cortex (Meunier et al., 1996; Murray and Mishkin, 1986). As a result, perirhinal cortex has three names and three different meanings in the current literature. Given that perirhinal cortex lies in the depths of two sulci (the rhinal sulcus anteriorly and the collateral sulcus anteriorly and posteriorly), and that perirhinal cortex has several names and designations, its location has been confounded with that of its neighbors. This complicated and convoluted scientific backdrop with respect to perirhinal is unfortunate, because imaging, cognitive, and behavioral neuroscientists rely on accurate neuroanatomical localization. When loose definitions occur anatomically, it is difficult to interpret functional findings and controversies can develop that are more semantic than substantive.

Regarding function, the perirhinal cortex plays a significant role in memory as has been demonstrated by several lines of evidence. Perirhinal cortex detects novel objects and denotes familiarity both in non-human primate studies and functional MRI (Buckley and Gaffan, 1998; Meunier et al., 1993, 1996; Murray and Mishkin, 1986; Murray et al., 2005; Suzuki et al., 1993; Zola-Morgan et al., 1989). The perirhinal cortex receives inputs from a plethora of diverse cortices and its strongest output is projected to the entorhinal cortex, its medial neighbor, (Suzuki and Amaral, 1994a,b; Van Hoesen and Pandya, 1975a), which in turn projects to the hippocampus (Van Hoesen and Pandya, 1975b). Undeniably, all of these structures, entorhinal, perirhinal and hippocampus are well known for their role in memory (Brown and Aggleton, 2001; Murray et al., 2005). In fact, when the memory circuit fails as it does in Alzheimer's disease, the medial temporal lobe reveals a burden of neurofibrillary tangles and beta-amyloid plaques (Arnold et al., 1991a; Braak and Braak, 1991). Moreover, perirhinal cortex manifests neurofibrillary tangles in normal aging and Alzheimer's disease (AD) at its earliest pathological stages in the MTL (Braak and Braak, 1985; Knopman et al., 2003; Kordower et al., 2001; Solodkin and Van Hoesen, 1996; Van Hoesen et al., 2000). As the disease progresses, neurofibrillary tangles and amyloid plaques dominate the entire cerebral cortical landscape, and replace healthy neurons with dysfunctional tangled ones and extracellular deposits (Arnold et al., 1991a; Braak and Braak, 1991). This massive neuronal cell death throughout MTL (and beyond in later stages) causes significant atrophy that has been detected with in vivo MRI. Several groups have demonstrated that entorhinal and perirhinal show volumetric changes between normal aging and mild Alzheimer's disease (De Toledo-Morrell et al., 2000; Jack et al., 1997; Kaye et al., 1997; Killiany et al., 2000, 2002; Xu et al., 2000) and the mesocortices represent the best indicators, and even more so, the predictors of converting to AD.

Currently, standard clinical MRI scans are acquired with voxels that are approximately 1–2 mm and are thus unable to resolve cortical architecture detail. A recent field has emerged called 'ex vivo imaging' where an autopsy brain is scanned allowing for the acquisition of ultra-high resolution images due to a number of factors that increase image SNR dramatically (e.g. no sample motion, optimal coil loading, exceptionally long scan sessions, reduced distance of the coils from the sample). Generating probabilistic maps based on ex vivo imaging has become a reliable method used to predict location and cortical boundaries because it can be validated with histological ground truth (Fischl et al., 2009). Ex vivo probability maps have improved upon global volumetric registration such as the Talairach atlas or relying on cortical folding patterns in an ad hoc manner, which can be problematic in higher order associative areas where the sulcal pattern is quite variable.

Our goal was to define the perirhinal cortex (area 35) in ex vivo MRI, validate the MRI-based labeling with Nissl staining, and build a probabilistic atlas for this area in FreeSurfer (http://surfer.nmr.mgh.harvard.edu/fswiki). In this study, we utilized probabilistic mapping based on high resolution ex vivo imaging to predict the location of the perirhinal cortex in the human brain, validated them with histological assays and applied our mesocortical (i.e. entorhinal and perirhinal) labels to the Alzheimer's Disease Neuroimaging Initiative (ADNI) dataset to assess cortical thickness in these vulnerable areas in the MTL in aging, mild cognitive impairment and Alzheimer's disease.

Materials and methods

Ex vivo samples

We collected 14 autopsied brain hemispheres from the Massachusetts General Hospital Autopsy Service (Massachusetts General Hospital, Boston MA) and the Framingham Heart Study and Boston University Alzheimer's Disease Center (Veterans Administration Medical Center, Bedford, VA). Each case was pathologically screened for overt neurological diagnoses such as strokes or significant atrophy and none was reported. Hemisphere laterality was evenly divided in our ex vivo sample set with seven left hemispheres and seven right hemispheres. The mean age was 66.9 years and standard deviation was 9.8 years. We procured 8 male and 2 female cases while in the remaining four cases gender information was unavailable. The post-mortem interval was restricted to be less than 25 h and our sample set had a mean PMI of 20.6 h and standard deviation of 5.6 h. Before scanning, each hemisphere was visually inspected for abnormalities and none were observed. These ex vivo cases were used for labeling and probabilistic mapping, as described in the following sections.

Radio frequency coils

We acquired images using two custom-made coils (Martinos Center for Biomedical Imaging, Charlestown MA) depending on whether we imaged the perirhinal cortex within a hemisphere or excised the MTL to create a block. For the hemispheres, we utilized a 4-channel phased array coil that consisted of 4 loop coil elements that were 5 cm in diameter and overlapped 1.5 cm with neighboring elements. The combined length of the 4 intertwining coils was approximately 16 cm. For the MTL blocks we utilized a 4-turn solenoid with a 28.5 mm inner diameter and 44 mm in length. For scanning, the hemisphere samples were packed in a plastic bag and vacuum sealed while the solenoid samples were packed in a plastic test tube (i.e. Falcon tube) and inserted into the solenoid holder.

Ex vivo imaging and acquisition

We used a fast low angle shot (FLASH) sequence on a 7.0 T human scanner from Siemens (Siemens Healthcare, Erlangen, Germany). Our standard resolution for the high resolution ex vivo samples was 120 μm isotropic for all cases except two cases where the resolution was 100 μm isotropic. We determined that a resolution of 120 μm in lieu of 100 μm still adequately revealed the relevant histoarchitectural (i.e. laminar) features with shortened scan time and increased SNR. We have optimized scan parameters in previous studies (Augustinack et al., 2005; Fischl et al., 2009) and found that a flip angle of 20° resulted in the best contrast to noise ratio per unit time. Furthermore, we set TR = 40 ms and TE = 20 ms and found that an echo time set at half the repetition time for ex vivo imaging produced consistent contrast quality and increased SNR when minimizing the bandwidth. It should be noted though that even though parameters were consistently controlled at standard settings, brain samples can yield various contrasts visually. In addition to the high resolution ex vivo images, we acquired MRI volumes of the entire brain hemispheres at a lower resolution, 1.0 mm × 1.0 mm × 1.0 mm so that we could create surface models and transform the label from the high resolution data to the lower resolution images for the purpose of creating the probabilistic maps for the perirhinal cortex based on spherical warping (Fischl et al., 1999a).

Neuroanatomical labeling

In previous studies (Fischl et al., 2009), we established a labeling protocol based on architectonic features observed in ex vivo MRI. We followed the topographical anatomy and cortical architecture described in previous reports (Braak and Braak, 1985; Ding and Van Hoesen, 2010; Van Hoesen et al., 2000). In this report, we labeled the perirhinal cortex, Brodmann's area 35, based on vertical modular columns in area 35a and an oblique wedge that is located between layers III–VI in area 35b. Lighter signal intensity was observed in neighboring ectorhinal (Brodmann area 36) along all cortical layers unlike the more superficial signal increase observed in perirhinal area 35. The perirhinal label described in this report will be publically released in FreeSurfer.

Terminology

The perirhinal cortex is a bipartite cortex composed of periallocortex for area 35a and proisocortex for area 35b (Sanides, 1969, 1970; Van Hoesen and Pandya, 1975a). This bipartite observation was first noticed by Sanides in the early 1970s (Van Hoesen and Pandya, 1975a) and carried forth by Van Hoesen et al. (2000) and colleagues (Ding and Van Hoesen, 2010). Mesocortex is a generic term that includes both periallocortex and proisocortex and that indicates the paralimbic belt of the cerebral cortex (Mesulam and Mufson, 1985; Pandya and Yeterian, 1985). This paralimbic or mesocortical belt of cortex intervenes between the three-layered (i.e. paleocortex or allocortex) cortex and the six-layered (i.e. neocortex, isocortex) cortex.

Registration

We used Register (MNI toolkit, Montreal, Canada, http://www.bic.mni.mcgill.ca) for all registrations that were performed in this study. We registered the FreeSurfer reconstructions to the higher resolution images that contained anatomical labels based on cortical architectural fields observed at ~120 μm. We used a 12-parameter affine registration in Register and manually set fiducial tags on corresponding points on the low and high resolution images, and used the correspondences to create a transform. This protocol was repeated for each case. After visual inspection, multiple registrations were performed using Register to refine and obtain the best possible registration. In ex vivo imaging, we, of course, have no head landmarks to ascertain customary coronal, axial and sagittal planes; thus, after MRI acquisition we rotated cases to a standard orientation and aligned them to our histological coronal plane. For the labeling, we occasionally observed sites that required manual editing of the high resolution labels (just editing a voxel or two voxels to account for errors sampling onto the surface) and these small edits did not significantly change the overall label. Given that the perirhinal primarily resides along the sulci, perirhinal labels were prone to "leaking" into abutting gray matter in the sulcus due to small mis-registration between the high resolution and low resolution volumes, necessitating a small amount of manual editing.

Participants and ADNI image acquisition

Data used in preparation of this article were obtained from the Alzheimer's Disease Neuroimaging Initiative (ADNI) database (www.loni.ucla.edu/ADNI) (Petersen et al., 2010). The ADNI was launched in 2003 by the National Institute on Aging, the National Institute of Biomedical Imaging and Bioengineering, the Food and Drug Administration, private pharmaceutical companies, and nonprofit organizations, as a $60-million, 5-year public–private partnership. The primary goal of ADNI is to test whether imaging measures, biological markers, and clinical and neuropsychological assessment can be combined to measure the progression of MCI and early AD. Detailed diagnostic, inclusion, and exclusion criteria are described on the ADNI Web site (http://www.adni-info.org/). Each participant gave written informed consent in accordance with institutional Human Subjects Research Committee guidelines.

MRI scans were collected on a 1.5 T scanner using a standardized magnetization-prepared rapid gradient echo protocol (Mugler and Brookeman, 1991): sagittal plane, repetition time/echo time/inversion time, 2400/3/1000 ms, flip angle 8°, 24 cm field of view, 192×192 in-plane matrix, 1.2 mm slice thickness (Jack et al., 2008).

We selected 740 subjects from the ADNI database that also produced good reconstructions from the FreeSurfer stream (FreeSurfer, Charlestown MA http://surfer.nmr.mgh.harvard.edu) (Dale et al., 1999; Fischl et al., 1999a,b, 2001; Segonne et al., 2004). All subjects were analyzed at baseline. The gender split included 436 males and 304 females. The diagnoses were normal controls (NC, n = 215), mild cognitive impairments (MCI, n = 358) and Alzheimer's disease (AD, n = 167). The mean age for the control group was 75.9 years with standard deviation 5.5 years while the mild cognitive impairment group had a mean age of 75.0 years with standard deviation 7.1 years and Alzheimer's group presented a mean age of 75.5 years with standard deviation 7.7 years. Thus, the three groups were age matched with a mean of approximately 75 years old. We used the FreeSurfer surfaces from these ADNI cases and our perirhinal and entorhinal labels to evaluate the cortical thickness in perirhinal and entorhinal cortices, respectively.

Statistics

For the cortical thickness analyses, we used a *t*-test in Matlab (Mathworks, Natick MA) to test the significance between the diagnoses (normal, mild cognitive impairment and Alzheimer's subjects). For each label, the vertices were ordered from most probable to least probable, then were thresholded so that the surface area of each predicted entorhinal cortex or perirhinal cortex label matched the average surface area of the ex vivo labels.

Results

Boundaries of perirhinal cortex

Several cortical architectural features defined the perirhinal cortex in MRI FLASH images. First, modularity was revealed by alternating light and dark intensity that was observed in the perirhinal area 35a. Second, dark signal was observed in the superficial layers in areas 35a and 35b, but this dark signal was only observed in infragranular layers in area 35a. Thus, the dark signal formed an oblique wedge throughout the anterior-posterior extent of the perirhinal cortex. The superficial layers of the perirhinal area 35b showed lighter intensity in the FLASH images compared to its inferior layers (i.e. layers IV (dysgranular), V, VI). The modularity and the wedge segment were consistently observed along the anterior-posterior axis and illustrated in one sample case (Fig. 1). White arrowheads show medial and lateral borders of the perirhinal cortex. Anteriorly at the level of the primary olfactory cortex, we have demonstrated our first MRI slice with the perirhinal cortex. The vertical columns and disparity in contrast between supragranular and infragranular layers were observed on the lateral parahippocampal gyrus (at this particular anterior-posterior level) and also on the medial bank of the collateral sulcus (Fig. 1A). At the rostral boundary as well as the caudal boundary (shown later), the perirhinal occupied part of the parahippocampal gyrus surface so that it came into view on the exposed gyrus from the depths of the sulcal topography. Moving posteriorly, the perirhinal cortex is positioned more laterally and in the next illustrated MRI slice, we observed the perirhinal cortex in the medial bank of the collateral sulcus and it no longer resided on the parahippocampal surface (Fig. 1B). The complex sulcal pattern of the human brain routinely creates a unique topography of the perirhinal cortex for each individual. The lighter signal in superficial layers in area 35b and the subsequent

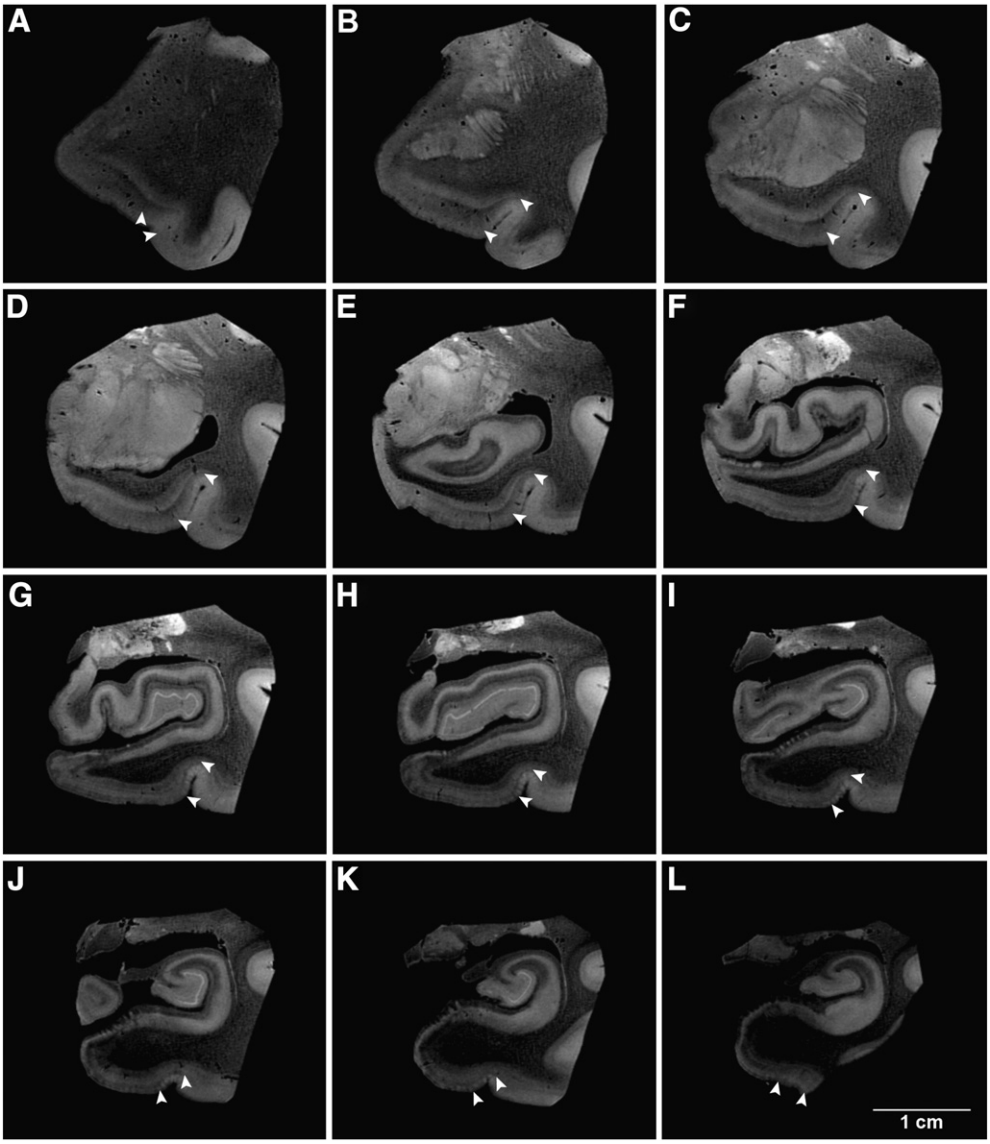

Fig. 1. Anterior-posterior coronal slices that demonstrate perirhinal cortex in ex vivo MRI. Several ex vivo MRI slices demonstrate detection of the perirhinal cortex (area 35) throughout its rostrocaudal extent in one selected case (67 year old, male). Note the vertical columnar structures in 35a and the oblique wedge in the entire area 35 that indicate the perirhinal cortex. White carets represent the medial and lateral borders in panels A–L.

wedge was a telltale sign of Brodmann's area 35b in ex vivo imaging. The perirhinal cortex continued in this location for several slices (Figs. 1C–F) and the bulk of perirhinal cortex resided on this medial bank. If the depth of collateral sulcus was shallow, we observed perirhinal cortex on the collateral sulcus medially but also found it overflowed slightly onto the lateral bank as well (Figs. 1G–I). In most of our cases, the perirhinal cortex obeyed the medial bank of the collateral sulcus and the fundus of the collateral sulcus marked the lateral boundary at this mid-rostrocaudal level. Nonetheless, when the sulcus was shallow or in the posterior perirhinal as the collateral sulcus ended, it was common for the perirhinal cortex to splay past the collateral fundus and slightly occupy the top of the lateral bank (Figs. 1J–K). The last panel (Fig. 1L) shows the perirhinal cortex positioned on the surface on the parahippocampal gyrus, posterior to where the entorhinal cortex ended. Posteriorly, the perirhinal ended approximately at the level of the lateral geniculate nucleus of the thalamus and ended in most cases as the collateral sulcus ended (but slightly more posterior about 1 mm, less than 10 MRI slices at 100 μm^3). Thus, the landmarks that defined the mediolateral boundaries changed slightly throughout the anterior-posterior extent of the parahippocampal gyrus. Perirhinal cortex extended beyond entorhinal cortex and encompassed the entorhinal cortex on all entorhinal sides, anteriorly, posteriorly and medially and was on the exposed parahippocampal surface at the anterior and posterior limits.

Histological-MRI validation of perirhinal cortex

We identified the perirhinal cortex, Brodmann's areas area 35, in high resolution ex vivo MRI and in Nissl stained histological sections. The Nissl stained sections were used to guide the detection of the cortical architectural ex vivo MRI features. The high resolution ex vivo MRI showed modularity in the superficial perirhinal cortex and layers II and III were organized into vertical columns (Fig. 2A). The vertical columns were evenly spaced and were present in area 35a. The medial border of the perirhinal cortex is adjacent to the entorhinal cortex and resides just inside the parahippocampal gyrus immediately medial to the collateral sulcus (Fig. 2). In this case, the border is not exactly on the bend of the parahippocampal crown but a few millimeters further inside the sulcus (within inset c in Fig. 2B). The depth of perirhinal columns depended on the depth of the collateral sulcus.

The example in Fig. 2 illustrates a fairly shallow collateral sulcus therefore the perirhinal columns exhibited relatively short columns (Fig. 2C). Nevertheless, the vertical columns displayed in close proximity to each other were visually distinct. Recognizably, the perirhinal columns showed greater depth than the entorhinal islands that only encompass layer II. Both the perirhinal columns and entorhinal islands were showed as bright intensities on ex vivo FLASH images (Fig. 2A). In this image, the brightness and contrast were optimized for the perirhinal cortex. The entorhinal cortex appears somewhat dim. Perirhinal area 35b lies more dorsally than perirhinal area 35a and was located closer to the collateral sulcus fundus (Figs. 2A and B). In its superficial layers, area 35b contains a wedge that has been described histologically (Braak and Braak, 1985) and we observed this oblique slant in ex vivo MRI and found it an extremely reliable feature in identifying the perirhinal cortex. The lateral border of the perirhinal cortex is adjacent to the ectorhinal cortex (Brodmann's area 36) and the boundary typically rests at the fundus of the collateral sulcus. In area 35b, the organization of the columns was not observed in the superficial layers, yet we observed the deep layers of area 35b demarcated by a dark region in ex vivo MRI as well as by histology (Fig. 2D). The oblique slant of this region was larger (vertically in the pia-white matter plane) in the more medial portion of 35b and narrowed laterally toward the fundus for area 35b. The area 35b—area 36 border showed differences in signal properties, with no oblique contrast in superficial layers but with bright signal intensity for these layers in ectorhinal area 36.

To validate what we observed in MRI, we demonstrated the cytoarchitectural organization in Nissl sections (Fig. 2B) and illustrated area 35a and area 35b on the medial bank of the collateral sulcus on this particular section. In this MTL block, many areas occupy this small region and in addition to the mesocortices, the hippocampus and subicular cortices show distinct cortical cellular organization. High magnification photomicrographs illustrate the laminar organization in the perirhinal cortex (Figs. 2C and D). Perirhinal area 35a and area 35b have a vastly different architecture as illustrated in Figs. 2C and D. Black arrows show the perirhinal columns while a single black arrowhead shows the lateral-most entorhinal island. The beginning of the wedge was demarcated with gray dotted lines in Fig. 2C for perirhinal area 35a and continued in Fig. 2D for perirhinal area 35b while the asterisk in Fig. 2D denotes layer V in area 35b.

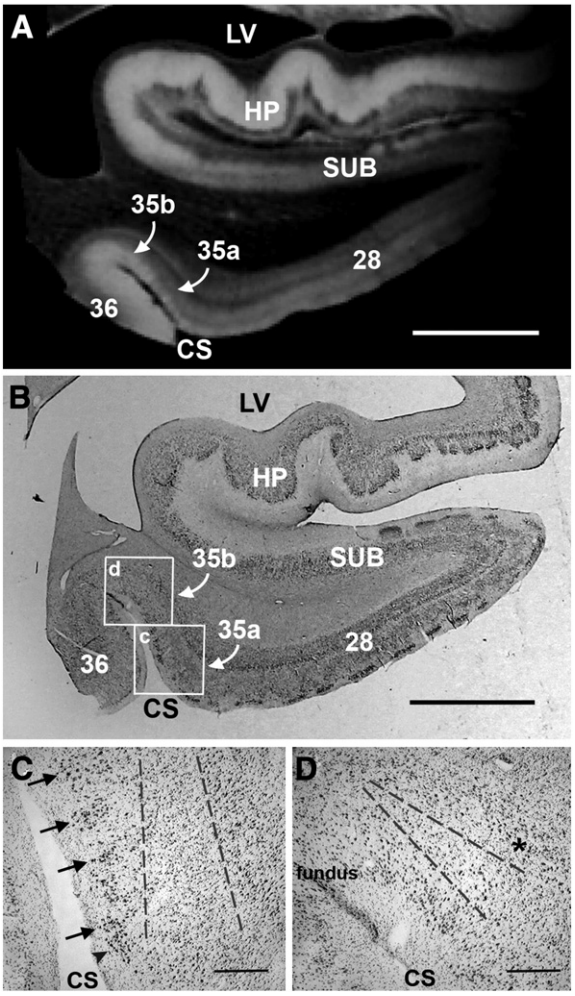

Fig. 2. Histological validation of the perirhinal cortex in ex vivo MRI. High resolution FLASH image (100 μm isotropic) that reveals columnar contrast in area 35a medially and lighter contrast superficially and laterally in area 35b in (A). The corresponding histological slice is illustrated in (B) with boxed insets for higher magnification photos of area 35a and area 35b respectively in (C) and (D). Black arrows point to the columns in perirhinal 35a and dotted lines in the infragranular lamina represent the medial portion of the oblique wedge observed in ex vivo MRI in (C). With the collateral sulcus fundus on the left, (D) shows the histological slice of area 35b and the lateral portion of the oblique wedge. The asterisk (*) denotes layer V in area 35b. Magnification bar = 5 mm in (A) and (B). Magnification bar = 500 μm in (C) and (D).

Perirhinal surface models

Two sets of MRI data were acquired, consisting of 1 mm^3 ex vivo data collected at 1.5 T and 100 μm isotropic ex vivo data collected at 7.0 T. The 1 mm^3 data was used to create a surface model for each individual case while the 100 μm data was used to delineate cortical lamina for the perirhinal cortex and demarcate perirhinal boundaries. Each case was manually labeled for the perirhinal cortex based on laminar observations in the high resolution ex vivo MRI. Once the entire extent of the perirhinal cortex was labeled, we manually registered the labeled high resolution data to the low resolution images and used a rigid transformation to move labels from high resolution to low resolution images. From that transformation, we generated individual maps for the left and right hemispheres (Fig. 3). The white label represents the perirhinal cortex (Brodmann's area 35) on the individual subject inflated surface maps.

To visualize the distance between labels, we used a common spherical coordinate system (Fischl et al., 1999a,b) and an existing template—fsaverage (FreeSurfer average)—to display a multiple subject spatial probability map in FreeSurfer. Each vertex on the average map was registered with vertices from each subject to determine colocalization of the perirhinal labels. Color labels (red and yellow) represent overlap within perirhinal labels whereas gray surface contains no perirhinal label (Fig. 4). Yellow represents 100% overlap, while gray represents 0% overlap of vertices. Dark and light gray correspond to cortical sulci and gyri, respectively. These probabilistic maps show the location of the perirhinal cortex in the anterior parahippocampal gyrus and more specifically that the perirhinal cortex is located in the medial bank of collateral sulcus and is also positioned on the parahippocampal surface at the anterior and posterior ends (Fig. 4). The probabilistic average for perirhinal area 35 is shown on an inflated fsaverage template.

Measurement and accuracy of surface models

To quantify the variability of the perirhinal cortex in our cases, we applied a modified symmetric Hausdorff distance (HD). The HD is a set theoretic measure that allows one to measure the “distance” between two point clouds. Typically the HD is defined as the maximum overall minimum distances between each point in one set to all the points in the other. This can be symmetrized by averaging the HD for the two directions (i.e. from set A to set B and from B to A). In addition, we have found the median to be a more stable measure than the maximum, so it is what we report here. The median HD was 4.0 mm for the left hemispheres (n = 7) and 3.2 mm for right hemispheres (n = 7) (Fig. 5) across subjects (that is, transforming each

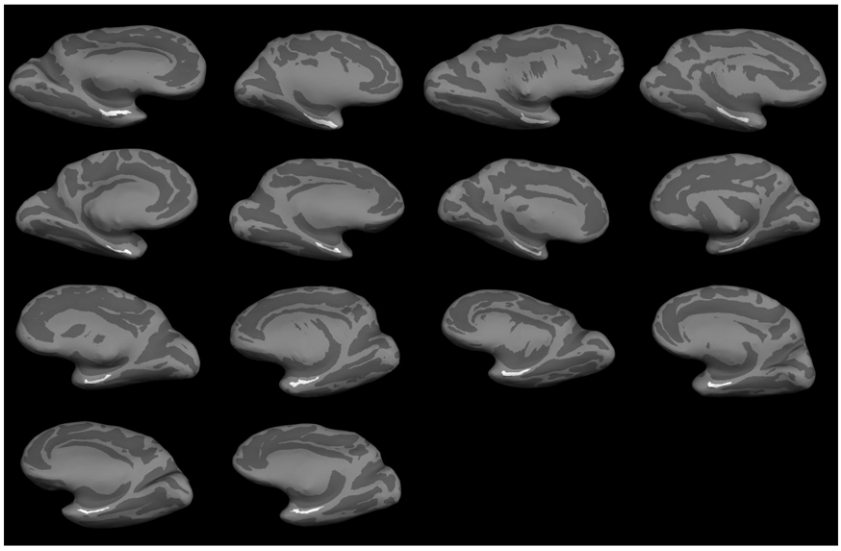

Fig. 3. Fourteen cases were labeled on high resolution ex vivo MRI volumes and mapped to respective individual surface maps. Each inflated brain shows the location of the perirhinal cortex (area 35) for each case labeled in white.

subject's perirhinal label through the spherical mapping, to every other subject, then computing the HD between the manual and the mapped labels). The left hemisphere showed slightly more variability than the right hemisphere.

Application of perirhinal surface models

To demonstrate the utility of the probabilistic mapping, we applied our probabilistic localization to a subset of ADNI participants. We limited the ADNI image volumes to datasets that contained good quality reconstructions and accurate spherical registration. We examined the cortical thickness in the perirhinal cortex (defined as area 35) and entorhinal cortex (defined as area 28) in the selected ADNI dataset of normal controls, (NC, n = 215, mean age = 75.9 years ± 5.5), mild cognitive impairment (MCI, n = 358, mean age = 75.0 years ± 7.1) and Alzheimer's disease (AD, n = 167, mean age = 75.5 years ± 7.7). The cortical thickness was larger for the control group in both predicted locations of the perirhinal and entorhinal cortices. The perirhinal cortex (black bars, Fig. 6) was slightly smaller than the entorhinal cortical in thickness (gray bars, Fig. 6) and with each diagnostic increment of disease (NC > MCI > AD). Thus, the cortical thickness was smaller in MCI and AD compared to normal controls (Fig. 6). Error bars stand for standard error of the mean for each group. Perirhinal thickness in normal controls was approximately 3.15 mm and decreased with MCI diagnosis to 2.8 mm and to 2.5 mm in AD in the left hemispheres. The same pattern was observed in the right hemisphere where controls showed a cortical thickness of 3.15 mm, MCI patients showed 2.8 mm and AD patients showed 2.5 mm. The differences were highly statistically different among each diagnostic group ($p<1.0^{-9}$ and $t<1.0^{-15}$). A similar progressive degenerative cortical thickness pattern was observed in the entorhinal cortex on the right and left but the entorhinal cortex thickness was slightly larger by approximately 0.2 mm–0.4 mm. These results suggest an accurate means to evaluate atrophy in MTL structures.

Discussion

In this report, we identified the location of the perirhinal cortex (Brodmann's area 35) using high resolution ex vivo MRI, validated the perirhinal cortex with histological analysis and applied surface based registration to our labeled perirhinal cortices to quantify the variability between subjects. We then utilized the labels to predict perirhinal cortex location in ADNI in vivo subjects and applied it to determine cortical thickness in controls, mild cognitive impairment patients and AD patients in Brodmann's area 35.

The perirhinal cortex (area 35) has similarities and differences from its neighboring regions, the entorhinal cortex (area 28) and isocortical area 36. Modularity or a clustering of neurons in the superficial layers is typically observed in entorhinal area 28 and perirhinal area 35a and has been referred to as entorhinal islands and perirhinal columns, respectively. The modularity in the perirhinal cortex includes not only layer II but also layer III, so that layers II–III make up the vertical column (Braak and Braak, 1985; Solodkin and Van Hoesen, 1996; Van Hoesen

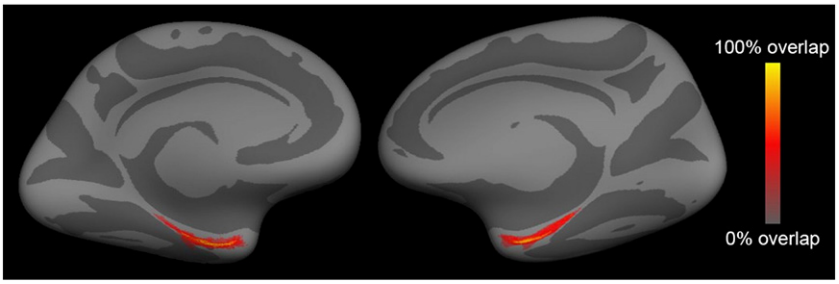

Fig. 4. Average probabilistic maps for the perirhinal cortex. Each case label was mapped onto an existing template—fsaverage—where labels overlapped to show high probability of localization in this ventromedial view. Yellow represents 100% overlap among cases.

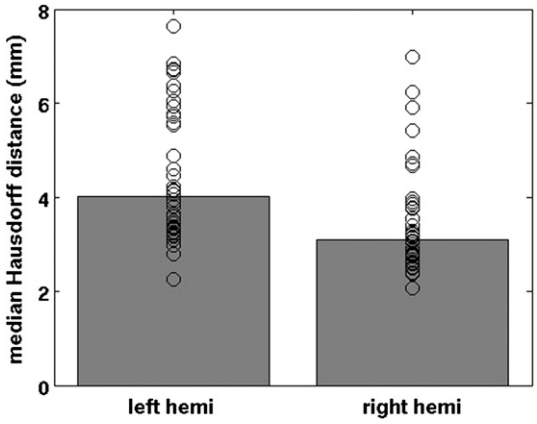

Fig. 5. Median Hausdorff distance in the perirhinal cortex. The Hausdorff distance was computed from the manual labels and the mapped label. The mean distance was 4.0 mm for the left hemisphere and 3.2 mm for the right hemisphere and the Hausdorff distance was slightly more variable in the left than right hemispheres.

and Solodkin, 1993; Van Hoesen et al., 2000). This modularity observed in area 28 and area 35a is a classic attribute of the periallocortex tissue type. Perirhinal area 35a is an agranular cortex which means that layer IV is absent. More specifically, a placeholder layer occurs spatially in layer IV but with no cells present. Perirhinal area 35b is a proisocortex with a dysgranular layer IV, which means that it has a few cells in layer IV but not completely organized yet. The organization of layer IV is one of the major differences between area 35 and area 36 (Ding and Van Hoesen, 2010; Ding et al., 2009; Insausti et al., 1998; Sanides, 1969). While area 35 is agranular and dysgranular (35a and 35b, respectively), area 36 contains a compact and granular layer IV. Layer V has medium sized pyramidal neurons in perirhinal areas 35a and 35b, but layer V in 35b is more organized and uniform compared to area 35a. Layer V in area 35b starts to resemble the internal pyramidal layer of isocortical areas but is not as thick, typically only one or two neurons. Layers V and VI are positioned closely together in the entorhinal, perirhinal and ectorhinal cortices. Thus, area 35 is periallocortex and proisocortex with agranular and dysgranular lamination patterns, respectively, while area 36 is isocortex because it has a distinct and granular layer IV (Gloor, 1997; Sanides, 1969; Stephan, 1975). Area 36

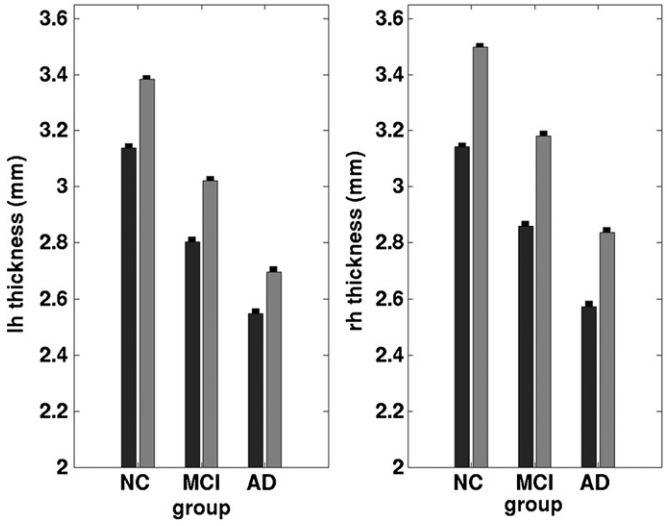

Fig. 6. Cortical thickness measures for ADNI subjects in the left and right hemispheres in controls, mild cognitive impairment and Alzheimer's disease. The black bars represent the perirhinal cortex (area 35) and the gray bars represent the entorhinal cortex (area 28). Note that the perirhinal cortex is thinner than the entorhinal cortex in each group but shows the same pattern of atrophy as the entorhinal cortex. Error bars represent standard error of the mean for each group.

contains all the components that quintessentially define the isocortex proper—thick layer I, granular layer IV, pyramidal neurons in layers III and V (Ding and Van Hoesen, 2010; Ding et al., 2009; Gloor, 1997; Insausti et al., 1998; Sanides, 1969; Stephan, 1975; Suzuki and Amaral, 2003a,b). Area 35 and area 36 also reveal distinct and different staining in immunocytochemical labeling in calcium binding proteins (calbindin-Dk28, parvalbumin), non-phosphorylated neurofilament protein (SMI-32), Wisteria floribunda agglutinin, and phosphorylated tau (AT8) (Ding and Van Hoesen, 2010).

As mentioned in the introduction, a confusing nomenclature has burdened the perirhinal cortex and contributed to its mis-localization. Brodmann described the perirhinal cortex as a "transitional cortex between archipallium and neopallium" (Brodmann, 1909; Brodmann and Garey, 1994) and while this may be, it saddled the perirhinal cortex with a poor connotation. Braak continued this by coining the term 'transentorhinal' cortex for perirhinal area 35 (Braak and Braak, 1985) and others have followed (Taylor and Probst, 2008). Brodmann also described perirhinal cortex as "[consisting] of a narrow strip-like zone limited to the rhinal sulcus and its immediate surroundings that follows this sulcus along its whole length, extending a little beyond it caudally" (Brodmann, 1909; Brodmann and Garey, 1994). Brodmann underestimated the size of perirhinal area 35. In fact, the perirhinal cortex (area 35) may be slightly larger than the entorhinal cortex (area 28) because perirhinal surrounds entorhinal on three sides (medially, anteriorly, and posteriorly) but this size depends on the sulcal depth. The nomenclature has been further complicated since several studies have grouped area 35 (perirhinal) and area 36 (ectorhinal) together (Ding and Van Hoesen, 2010; Insausti et al., 1998; Suzuki and Amaral, 1994a,b). The grouping of area 35 and area 36 was an unfortunate event but likely occurred due to non-human primate studies where it was difficult to target only one Brodmann area, or there was similar connectivity (e.g. Suzuki and Amaral argued that areas 35 and 36 produced similar connectivity in macaque but included area TE in their explanation) (Suzuki and Amaral, 1994a), differences in evolutionary animal anatomy, or misidentification due to confusing sulcal patterns. It may even be that the term ectorhinal was dismissed because it is too similar in spelling to entorhinal with just one letter difference between them. It is important to note that areas 36 and 20 (visual association areas) correspond approximately to visually dominant areas (TE of von Economo) (von Economo and Koskinas, 1925), which are isocortical areas while the perirhinal cortex (area 35) is a periallocortical–proisocortical multimodal area. Several additional studies have categorized area 28 and area 35 together as rhinal cortex. The mesocortices may have been grouped for similar reasons as described above, or due to an inclination to keep continuity with the rodent brain. Thus, categorically, the perirhinal cortex has been merged with the entorhinal cortex medially (i.e. rhinal cortex) (Meunier et al., 1993; Murray and Mishkin, 1986) or with the ectorhinal cortex (area 36) laterally (Ding and Van Hoesen, 2010; Insausti et al., 1998; Suzuki and Amaral, 1994b), but also alone (Solodkin and Van Hoesen, 1996; Van Hoesen and Pandya, 1975b; Van Hoesen and Solodkin, 1993; Van Hoesen et al., 2000).

Teasing out area 35 analyses from previous studies that have merged perirhinal area 35 with other above mentioned areas (entorhinal or area 36), our MRI detection of the perirhinal cortex agrees with Ding and Van Hoesen (2010) and Insausti et al. (1998) for the anterior-posterior extent for area 35 analyses only in that it extends from the temporal incisura anteriorly to slightly past the level of the lateral geniculate nucleus of the thalamus posteriorly. Moreover, we determined that Sanides' anatomical description of 35a and 35b was the most consistent with our ex vivo MRI and corresponding Nissl analysis. Our results also agree with Braak and Braak (1985) and Van Hoesen et al. (2000) regarding the medial-lateral boundaries among areas 28, 35 and 36. Due to the location of the perirhinal cortex spanning two gyri, multiple names have emerged. Insausti described 35v and 35o where ventral area 35 roughly corresponds to anterior area 35 at the temporal incisura (Insausti et al., 1998) and Insausti's 35o represents area 35

oblique and corresponds to the bulk of area 35, along the medial bank of the collateral sulcus, (i.e. Braak's transentorhinal) (Braak and Braak, 1985; Ding and Van Hoesen, 2010; Van Hoesen and Solodkin, 1993). These studies also noted the columnar regions (area 35a) and oblique wedge in the lateral perirhinal cortex (area 35b). Our ex vivo MRI images revealed this pattern and displayed the oblique pattern anteriorly, aligned on the medial bank of the collateral sulcus at the level of the amygdala, and continuing posteriorly until the sulcus ends.

It could be postulated whether the architecture of perirhinal area 35 represents a distinct pattern, or is a continuum between the entorhinal and ectorhinal (area 36) cortices. Based on the fact that perirhinal's architecture is consistent from brain to brain, our data and others' support a specific pattern for the perirhinal cortex, although there may be some truth to the continuum perspective as well. It could be a continuum because it contains features that resemble the entorhinal cortex medially and temporal isocortex (area 36) laterally. The former description—a specific pattern—is preferred due to the distinct cortical architecture and the considerable size of area 35. Our probabilistic map of the perirhinal cortex rivals the size of our probabilistic map for the entorhinal cortex (Fischl et al., 2009) and this agrees with others that have shown the extensive size of the perirhinal cortex (Braak, 1980; Ding and Van Hoesen, 2010; Insausti et al., 1998). Given that the mesocortical (i.e. paralimbic) belt intervenes between the allocortex and isocortex, transitional cortices have been observed with retrosplenial cortex as well with a different pattern (Braak, 1980), which argues for the condition that the perirhinal cortex exhibits a specific pattern of cortical architecture. We recommend referring to area 36 as 'isocortical area 36' and only using the term perirhinal cortex to refer to area 35 in future publications.

Several studies have investigated the relationship between myelin content and ex vivo contrast (Augustinack et al., 2010; Bock et al., 2009; Eickhoff et al., 2005; Geyer et al., 2011). In ex vivo MRI of fixed tissue, a variety of contrasts have been reported that correlate with myelin content, T2* (Fukunaga et al., 2010), T2 (Augustinack et al., 2010; Eickhoff et al., 2005) as well as T1 (Bock et al., 2009; Geyer et al., 2011) and the phase (susceptibility weighted) (Duyn et al., 2007; Langkammer et al., 2012). The medial temporal lobe and in particular the entorhinal and perirhinal cortices are not generally heavily myelinated with the exception of the alveus and the molecular layer of the presubiculum (the superficial presubicular pathway) (Rosene and Van Hoesen, 1987). Nonetheless, myeloarchitecture in perirhinal cortex provides excellent ex vivo contrast. Braak described and illustrated the cyto-, pigmento- (relating to lipofuscin granules) and myeloarchitecture of the temporal lobe (Braak, 1980; Braak and Braak, 1985) and from his illustrations, one can observe the oblique wedge of the dark signal in areas 35a and 35b that we observed in ex vivo MRI. The illustrations of Krimer and colleagues also resemble, quite remarkably, the oblique pattern in area 35 (Krimer et al., 1997). Krimer's Gallyas staining appears so similar to our images that it is difficult to discern which is ex vivo MRI and which is Gallyas staining when viewed side by side. Insausti and colleagues (Insausti et al., 1995) also showed myelin staining in this region as well as Nissl staining where the oblique pattern in the perirhinal cortex was observed in both stains, similarly noted in Braak's publications (Braak, 1980; Braak and Braak, 1985). The pattern in the Nissl stain, albeit more subtle in some cases, may require a neuroanatomically trained eye to appreciate. The ex vivo MRI contrast observed in the perirhinal cortex, particularly in the oblique wedge, has a cyto-, pigmento-, and myeloarchitectural basis (Braak, 1980; Eickhoff et al., 2005; Krimer et al., 1997). Eickhoff and colleagues provided quantitative evidence for the concept that it was a mixture of contrast but that myelin contributed more than other properties to the observed MRI intensities (Eickhoff et al., 2005). Ex vivo validation will continue to play an important role in understanding MRI contrast and underlying myeloarchitecture in the human brain. The myeloarchitecture distribution and specificity of known pathways, bundles and cortical areas will validate in vivo studies and help determine sequences and contrast that corroborate ex vivo findings with in vivo "myelin content", such as T1w/T2w ratio (Glasser and Van Essen, 2011), reciprocal of T1 (Sigalovsky et al., 2006) and decreased T2* in myelinated area (Cohen-Adad et al., 2012; van Gelderen et al., 2012) or increased T2* in demyelinated conditions (Lee et al., 2012).

The sulcal pattern in the MTL has also complicated the understanding of area 35 because the sulcal configurations vary considerably from human brain to human brain (Hanke, 1997; Insausti et al., 1995; Ono et al., 1990; Van Hoesen, 1995; Van Hoesen et al., 2000). The collateral sulcus is variable in length and depth, and at least 5 common patterns have been documented (non-interrupted, interrupted, interrupted but connected, interrupted and overlapped, multiple interruptions) (Bobinski et al., 1999; de Leon et al., 2004; Feczko et al., 2009; Goncharova et al., 2001; Hanke, 1997; Insausti et al., 1995, 1998; Van Hoesen, 1995). The variability of the collateral sulcus together with similar, and arguably worse, variability in the incipient rhinal sulcus creates confusion for the identification of the underlying cortex that runs along both of these sulci, perirhinal cortex (area 35). It is important to emphasize that we labeled based on laminar features and not sulcal topography. Nonetheless, sulcal topography is worthy of discussion because so many studies define these two sulci and perirhinal incorrectly. Depending on the sulcal depth, perirhinal cortex can be larger than the entorhinal cortex because it surrounds entorhinal on all sides, except for entorhinal's anterior border with primary olfactory cortex. Perirhinal cortex (area 35) spans two sulci (rhinal and collateral) and two gyri (anterior lateral temporal cortex and parahippocampal). In this study, we define the rhinal sulcus as completely separate from the collateral sulcus (Braak and Braak, 1992; Ono et al., 1990; Suzuki and Amaral, 1994a; Van Hoesen, 1995; Van Hoesen et al., 2000) and do not ascribe to the rhinal sulcus being the anterior part of the collateral (Hanke, 1997). The sulcal boundaries for the entorhinal and perirhinal cortices can be elaborate, but in the most simple terms, a rhinal sulcus borders anteriorly and the collateral sulcus borders laterally. The entorhinal cortex lies medially, well within the boundaries of both sulci, on the crown of the anterior parahippocampal gyrus. The topography of the perirhinal cortex is where the complexity is introduced because it resides in the depths of both sulci (rhinal and collateral) but on different banks in each. Perirhinal area 35 is positioned lateral to the rhinal sulcus but also medial to the collateral sulcus. Thus, perirhinal cortex is on the lateral bank of the rhinal sulcus and on the medial bank of the collateral sulcus. Perirhinal's location on the lateral bank of the rhinal sulcus in the human brain agrees with the position of the perirhinal cortex in non-human primates but the location on the medial bank of the collateral sulcus is unique to the human brain. The rhinal sulcus is absent in many human brains and is sometimes represented by a subtle groove or nothing at all, which is why it is often dubbed incipient. The collateral sulcus is more dependable and is routinely observed lateral to the entorhinal cortex and perirhinal area 35. Moreover, these complicated folding patterns such as the collateral and rhinal sulcus and intervening cortex, create problems for other registration or localization methods such as registration to a single template volume (i.e. Talairach volume), which may yield poor localization and poor accuracy because all common sulcal patterns were not represented. With ex vivo probabilistic mapping, multiple sulcal patterns are statistically summarized at multiple spatial scales and nearby sulci can help with localization of architectonics if the boundaries are consistent distances from stably occurring folds. This becomes important when research studies report that the right rhinal sulcus pattern was underrepresented in AD (Zhan et al., 2009), but given that the rhinal sulcus is extremely variable in humans and often it is so shallow that it is hardly a sulcus but instead a groove anteriorly, it is possible that the label was limited to the collateral sulcus. In contrast, the utilization of high resolution ex vivo labeling with the ability to assess cortical brain areas regardless of sulcal pattern, enables an accurate localization of the perirhinal cortex. Cortical areas that occupy the depths of a sulcus and not the

crown of a gyrus have not been well studied or localized due to previous technical limitations. The study of brain function depends on accurate and specific localization of anatomical areas, and lack of that—specificity and accuracy—can create a confounding factor in many studies. Our method and localization of the perirhinal cortex provides a prototypical example of mapping areas that are hidden to an exterior observer (i.e. in sulcal depths).

Although this topic may seem like neuroanatomical minutiae, defining each area in the human brain becomes extremely important when diagnosing or predicting diagnoses or conversion to Alzheimer's disease, because these mesocortical areas in the MTL are the most vulnerable to NFT pathology in aging and AD. Area 35 and area 36 exhibit different pathological grades and at different times in the disease progression (Braak and Braak, 1991). Neurons in area 36 atrophy much later in the disease compared to area 35, which is the first area to display neurofibrillary tangles in aging and AD (Arnold et al., 1991b; Braak and Braak, 1991; Kemper, 1984; Knopman et al., 2003; Kordower et al., 2001; Van Hoesen et al., 2000). Others have used cortical thickness measures to illustrate more explicitly that the cortical ribbon is degenerating in these regions at an early stage (Dickerson et al., 2009a,b, 2011) and likely reflects pathological cerebral atrophy. Our results showed differences between entorhinal cortical thickness and perirhinal cortical thickness in controls, MCI and AD patients and this method provides a more specific metric with area 35 alone than all medial temporal areas together. Furthermore, our tool allows mapping of perirhinal area 35 that has been validated with cortical architecture (i.e. histoarchitecture). Further analyses of cortical thickness were assessed and perirhinal exhibited the same composition as entorhinal cortex with significant thinning in MCI and AD patients. Thus, MRI techniques have improved from a global atrophy measurement to now pinpointing specific areas, and this improvement may reflect and more accurately correlate with behavioral and cognitive scores in future studies.

Analogous to how anatomical definitions can confound disease-related analyses; functional consequences may be confounded as well. Animal and functional imaging studies have shown that perirhinal cortex detects novel objects, is required for object recognition, and forms an abstract representation of the object shown with delayed match and delayed non-match experiments, suggesting a role in memory (Barense et al., 2010; Brown and Aggleton, 2001; Buffalo et al., 2006; Murray and Mishkin, 1998; Murray et al., 2005). Thus, perirhinal cortex reveals activation when an object is novel and predicts familiarity-based recognition memory responses. Lesions of the perirhinal in macaques have confirmed this novel detection of objects (Buckley and Gaffan, 1998; Murray and Mishkin, 1986; Suzuki et al., 1993; Zola-Morgan et al., 1989). A controversy exists regarding whether perirhinal cortex is involved in object recognition or object perception (Hampton, 2005; Murray et al., 2000). Imprecise anatomical definitions or grouping multiple areas are commonly proliferated in functional imaging studies. Devlin et al. argue that the perirhinal cortex is involved in visual perception and also in memory and language (Devlin and Price, 2007). This raises the question: is this the case because humans rely mainly on visual input, or is it because the anatomical area defined was large (area 35 + area 36) and included a substantial visual associative area (isocortical area 36)? Cognitive neurobiologists have noted the controversy where Hampton outlined the problems that arose from methodological distinctions regarding perception and memory (Buckley and Gaffan, 1998; Hampton, 2005). Perhaps careful fMRI studies that explicitly define the perirhinal as area 35 only can distinguish more a specific function for the perirhinal and distinguish it from surrounding cortices. Our probabilistic mapping provides an accurate localization of the perirhinal cortex and may help future application studies define area 35, and further characterize its functional properties. Functional MRI, and behavioral or cognitive studies are predicated on accurate anatomical localization and when a precise localization does not occur, results can be confounded and difficult to interpret.

Conclusion

Understanding cortical areas that traverse more than one gyrus or sulcus is an important task and critical in the assessment of normal brain function as well as disease states. Several imaging studies have utilized a volumetric approach to evaluate and predict the state of atrophy in the MTL in AD. As quantitative measures evolve in imaging from global atrophy to specific metrics such as cortical thickness, it is important to accurately assess each anatomical area in healthy controls, non-demented aging and AD, as well as other neurodegenerative disorders. Our ex vivo probabilistic mapping of the perirhinal cortex provides significant benefits in this endeavor in the form of specific, histologically validated, automated and accurate labeling of architectonic regions in the MTL, facilitating the analysis of atrophic change in a large dataset for earlier detection and diagnosis of the many diseases that affect the MTL. Refined detection of individual areas will enable accurate localization and assessment of smaller, more homogeneously affected brain areas, facilitating earlier detection of disease processes, and enhancing the possibility of therapeutic intervention before widespread cell death.

Acknowledgments

We would like to thank those who donated tissue; their generous donation made this work possible. We extend special thanks to Brad Dickerson for reading this manuscript and helpful comments. Support for this research was provided in part by the National Center for Research Resources (P41-RR14075, and the NCRR BIRN Morphometric Project BIRN002, U24 RR021382), the National Institute for Biomedical Imaging and Bioengineering (R01EB006758), the National Institute on Aging (AG022381) and (AG028521), the Massachusetts (MGH) Alzheimer's Disease Resource Center (5P50AG005134-28), Boston University Alzheimer's Disease Center and Framingham Heart Study (P30-AG13846 and R01 AG1649), the National Center for Alternative Medicine (RC1AT005728-01), the National Institute for Neurological Disorders and Stroke (R01 NS052585-01, 1R21NS072652-01, 1R01NS070963), and was made possible by the resources provided by Shared Instrumentation Grants 1S10RR023401, 1S10RR019307, and 1S10RR023043. Additional support was provided by The Autism & Dyslexia Project funded by the Ellison Medical Foundation and by the NIH Blueprint for Neuro-science Research (U01-MH093765, part of the multi-institutional Human Connectome Project). Data collection and sharing for this project was funded by the Alzheimer's Disease Neuroimaging Initiative (ADNI) (National Institutes of Health Grant U01 AG024904). ADNI is funded by the National Institute on Aging, the National Institute of Biomedical Imaging and Bioengineering, and through generous contributions from the following: Abbott; Alzheimer's Association; Alzheimer's Drug Discovery Foundation; Amorfix Life Sciences Ltd.; AstraZeneca; Bayer HealthCare; BioClinica, Inc.; Biogen Idec Inc.; Bristol-Myers Squibb Company; Eisai Inc.; Elan Pharmaceuticals Inc.; Eli Lilly and Company; F. Hoffmann-La Roche Ltd. and its affiliated company Genentech, Inc.; GE Healthcare; Innogenetics, N.V.; Janssen Alzheimer Immunotherapy Research & Development, LLC.; Johnson & Johnson Pharmaceutical Research & Development LLC.; Medpace, Inc.; Merck & Co., Inc.; Meso Scale Diagnostics, LLC.; Novartis Pharmaceuticals Corporation; Pfizer Inc.; Servier; Synarc Inc.; and Takeda Pharmaceutical Company. The Canadian Institutes of Health Research is providing funds to support ADNI clinical sites in Canada. Private sector contributions are facilitated by the Foundation for the National Institutes of Health (www.fnih.org). The grantee organization is the Northern California Institute for Research and Education, and the study is coordinated by the Alzheimer's Disease Cooperative Study at the University of California, San Diego. ADNI data are disseminated by the Laboratory for Neuro Imaging at the University of California, Los Angeles. This research was also supported by NIH grants P30 AG010129, K01 AG030514, and the Dana Foundation.

References

Arnold, S.E., Hyman, B.T., Flory, J., Damasio, A.R., Van Hoesen, G.W., 1991a. The topographical and neuroanatomical distribution of neurofibrillary tangles and neuritic plaques in the cerebral cortex of patients with Alzheimer's disease. Cereb. Cortex 1, 103–116.

Arnold, S.E., Hyman, B.T., Van Hoesen, G.W., Damasio, A.R., 1991b. Some cytoarchitectural abnormalities of the entorhinal cortex in schizophrenia. Arch. Gen. Psychiatry 48, 625–632.

Augustinack, J.C., van der Kouwe, A.J., Blackwell, M.L., Salat, D.H., Wiggins, C.J., Frosch, M.P., Wiggins, G.C., Potthast, A., Wald, L.L., Fischl, B.R., 2005. Detection of entorhinal layer II using 7 Tesla magnetic resonance imaging. Ann. Neurol. 57, 489–494.

Augustinack, J.C., Helmer, K., Huber, K.E., Kakunoori, S., Zollei, L., Fischl, B., 2010. Direct visualization of the perforant pathway in the human brain with ex vivo diffusion tensor imaging. Front. Hum. Neurosci. 4, 42.

Barense, M.D., Henson, R.N., Lee, A.C., Graham, K.S., 2010. Medial temporal lobe activity during complex discrimination of faces, objects, and scenes: effects of viewpoint. Hippocampus 20, 389–401.

Bobinski, M., de Leon, M.J., Convit, A., De Santi, S., Wegiel, J., Tarshish, C.Y., Saint Louis, L.A., Wisniewski, H.M., 1999. MRI of entorhinal cortex in mild Alzheimer's disease. Lancet 353, 38–40.

Bock, N.A., Kocharyan, A., Liu, J.V., Silva, A.C., 2009. Visualizing the entire cortical myelination pattern in marmosets with magnetic resonance imaging. J. Neurosci. Methods 185, 15–22.

Braak, H., 1980. Architectonics of the Human Telencephalic Cortex. Studies of Brain Function. Springer-Verlag, Berlin Heidleberg, pp. 42–48.

Braak, H., Braak, E., 1985. On areas of transition between entorhinal allocortex and temporal isocortex in the human brain. Normal morphology and lamina-specific pathology in Alzheimer's disease. Acta Neuropathol. 68, 325–332.

Braak, H., Braak, E., 1991. Neuropathological staging of Alzheimer-related changes. Acta Neuropathol. (Berl.) 82, 239–259.

Braak, H., Braak, E., 1992. The human entorhinal cortex: normal morphology and lamina-specific pathology in various diseases. Neurosci. Res. 15, 6–31.

Brodmann, K., 1909. Vergleichende Lokalisationslehre der Groshirnrinde. Verlag von Johann Ambrosius Barth, Leipzig.

Brodmann, K., Garey, L., 1994. Brodmann's Localisation in the Cerebral Cortex. Smith-Gordon, London.

Brown, M.W., Aggleton, J.P., 2001. Recognition memory: what are the roles of the perirhinal cortex and hippocampus? Nat. Rev. Neurosci. 2, 51–61.

Buckley, M.J., Gaffan, D., 1998. Perirhinal cortex ablation impairs visual object identification. J. Neurosci. 18, 2268–2275.

Buffalo, E.A., Bellgowan, P.S., Martin, A., 2006. Distinct roles for medial temporal lobe structures in memory for objects and their locations. Learn. Mem. 13, 638–643.

Cohen-Adad, J., Polimeni, J.R., Helmer, K.G., Benner, T., McNab, J.A., Wald, L.L., Rosen, B.R., Mainero, C., 2012. T(2)* mapping and B(0) orientation-dependence at 7 T reveal cyto- and myeloarchitecture organization of the human cortex. Neuroimage 60, 1006–1014.

Dale, A.M., Fischl, B., Sereno, M.I., 1999. Cortical surface-based analysis. I. Segmentation and surface reconstruction. Neuroimage 9, 179–194.

de Leon, M.J., DeSanti, S., Zinkowski, R., Mehta, P.D., Pratico, D., Segal, S., Clark, C., Kerkman, D., DeBernardis, J., Li, J., Lair, L., Reisberg, B., Tsui, W., Rusinek, H., 2004. MRI and CSF studies in the early diagnosis of Alzheimer's disease. J. Intern. Med. 256, 205–223.

De Toledo-Morrell, L., Goncharova, I., Dickerson, B., Wilson, R.S., Bennett, D.A., 2000. From healthy aging to early Alzheimer's disease: in vivo detection of entorhinal cortex atrophy. Ann. N. Y. Acad. Sci. 911, 240–253.

Devlin, J.T., Price, C.J., 2007. Perirhinal contributions to human visual perception. Curr. Biol. 17, 1484–1488.

Dickerson, B.C., Bakkour, A., Salat, D.H., Feczko, E., Pacheco, J., Greve, D.N., Grodstein, F., Wright, C.I., Blacker, D., Rosas, H.D., Sperling, R.A., Atri, A., Growdon, J.H., Hyman, B.T., Morris, J.C., Fischl, B., Buckner, R.L., 2009a. The cortical signature of Alzheimer's disease: regionally specific cortical thinning relates to symptom severity in very mild to mild AD dementia and is detectable in asymptomatic amyloid-positive individuals. Cereb. Cortex 19, 497–510.

Dickerson, B.C., Feczko, E., Augustinack, J.C., Pacheco, J., Morris, J.C., Fischl, B., Buckner, R.L., 2009b. Differential effects of aging and Alzheimer's disease on medial temporal lobe cortical thickness and surface area. Neurobiol. Aging 30, 432–440.

Dickerson, B.C., Stoub, T.R., Shah, R.C., Sperling, R.A., Killiany, R.J., Albert, M.S., Hyman, B.T., Blacker, D., Detoledo-Morrell, L., 2011. Alzheimer-signature MRI biomarker predicts AD dementia in cognitively normal adults. Neurology 76, 1395–1402.

Ding, S.L., Van Hoesen, G.W., 2010. Borders, extent, and topography of human perirhinal cortex as revealed using multiple modern neuroanatomical and pathological markers. Hum. Brain Mapp. 31, 1359–1379.

Ding, S.L., Van Hoesen, G.W., Cassell, M.D., Poremba, A., 2009. Parcellation of human temporal polar cortex: a combined analysis of multiple cytoarchitectonic, chemoarchitectonic, and pathological markers. J. Comp. Neurol. 514, 595–623.

Duyn, J.H., van Gelderen, P., Li, T.Q., de Zwart, J.A., Koretsky, A.P., Fukunaga, M., 2007. High-field MRI of brain cortical substructure based on signal phase. Proc. Natl. Acad. Sci. U. S. A. 104, 11796–11801.

Eickhoff, S., Walters, N.B., Schleicher, A., Kril, J., Egan, G.F., Zilles, K., Watson, J.D., Amunts, K., 2005. High-resolution MRI reflects myeloarchitecture and cytoarchitecture of human cerebral cortex. Hum. Brain Mapp. 24, 206–215.

Feczko, E., Augustinack, J.C., Fischl, B., Dickerson, B.C., 2009. An MRI-based method for measuring volume, thickness and surface area of entorhinal, perirhinal, and posterior parahippocampal cortex. Neurobiol. Aging 30, 420–431.

Fischl, B., Sereno, M.I., Dale, A.M., 1999a. Cortical surface-based analysis. II: inflation, flattening, and a surface-based coordinate system. Neuroimage 9, 195–207.

Fischl, B., Sereno, M.I., Tootell, R.B., Dale, A.M., 1999b. High-resolution intersubject averaging and a coordinate system for the cortical surface. Hum. Brain Mapp. 8, 272–284.

Fischl, B., Liu, A., Dale, A.M., 2001. Automated manifold surgery: constructing geometrically accurate and topologically correct models of the human cerebral cortex. IEEE Trans. Med. Imaging 20, 70–80.

Fischl, B., Stevens, A.A., Rajendran, N., Yeo, B.T., Greve, D.N., Van Leemput, K., Polimeni, J.R., Kakunoori, S., Buckner, R.L., Pacheco, J., Salat, D.H., Melcher, J., Frosch, M.P., Hyman, B.T., Grant, P.E., Rosen, B.R., van der Kouwe, A.J., Wiggins, G.C., Wald, L.L., Augustinack, J.C., 2009. Predicting the location of entorhinal cortex from MRI. Neuroimage 47, 8–17.

Fukunaga, M., Li, T.Q., van Gelderen, P., de Zwart, J.A., Shmueli, K., Yao, B., Lee, J., Maric, D., Aronova, M.A., Zhang, G., Leapman, R.D., Schenck, J.F., Merkle, H., Duyn, J.H., 2010. Layer-specific variation of iron content in cerebral cortex as a source of MRI contrast. Proc. Natl. Acad. Sci. U. S. A. 107, 3834–3839.

Geyer, S., Weiss, M., Reimann, K., Lohmann, G., Turner, R., 2011. Microstructural parcellation of the human cerebral cortex—From Brodmann's post-mortem map to in vivo mapping with high-field magnetic resonance imaging. Front. Hum. Neurosci. 5, 19.

Glasser, M.F., Van Essen, D.C., 2011. Mapping human cortical areas in vivo based on myelin content as revealed by T1- and T2-weighted MRI. J. Neurosci. 31, 11597–11616.

Gloor, P., 1997. The Temporal Lobe and Limbic System. Oxford University Press, New York, New York.

Goncharova, I.I., Dickerson, B.C., Stoub, T.R., deToledo-Morrell, L., 2001. MRI of human entorhinal cortex: a reliable protocol for volumetric measurement. Neurobiol. Aging 22, 737–745.

Hampton, R.R., 2005. Monkey perirhinal cortex is critical for visual memory, but not for visual perception: reexamination of the behavioural evidence from monkeys. Q. J. Exp. Psychol. B 58, 283–299.

Hanke, J., 1997. Sulcal pattern of the anterior parahippocampal gyrus in the human adult. Ann. Anat. 179, 335–339.

Insausti, R., Tunon, T., Sobreviela, T., Insausti, A.M., Gonzalo, L.M., 1995. The human entorhinal cortex: a cytoarchitectonic analysis. J. Comp. Neurol. 355, 171–198.

Insausti, R., Juottonen, K., Soininen, H., Insausti, A.M., Partanen, K., Vainio, P., Laakso, M.P., Pitkanen, A., 1998. MR volumetric analysis of the human entorhinal, perirhinal, and temporopolar cortices. AJNR Am. J. Neuroradiol. 19, 659–671.

Jack Jr., C.R., Petersen, R.C., Xu, Y.C., Waring, S.C., O'Brien, P.C., Tangalos, E.G., Smith, G.E., Ivnik, R.J., Kokmen, E., 1997. Medial temporal atrophy on MRI in normal aging and very mild Alzheimer's disease. Neurology 49, 786–794.

Jack Jr., C.R., Bernstein, M.A., Fox, N.C., Thompson, P., Alexander, G., Harvey, D., Borowski, B., Britson, P.J., J, L.W., Ward, C., Dale, A.M., Felmlee, J.P., Gunter, J.L., Hill, D.L., Killiany, R., Schuff, N., Fox-Bosetti, S., Lin, C., Studholme, C., DeCarli, C.S., Krueger, G., Ward, H.A., Metzger, G.J., Scott, K.T., Mallozzi, R., Blezek, D., Levy, J., Debbins, J.P., Fleisher, A.S., Albert, M., Green, R., Bartzokis, G., Glover, G., Mugler, J., Weiner, M.W., 2008. The Alzheimer's Disease Neuroimaging Initiative (ADNI): MRI methods. J. Magn. Reson. Imaging 27, 685–691.

Jones, E.G., Powell, T.P.S., 1970. An anatomical study of converging sensory pathways within the cerebral cortex of the monkey. Brain 93, 793–820.

Kaye, J.A., Swihart, T., Howieson, D., Dame, A., Moore, M.M., Karnos, T., Camicioli, R., Ball, M., Oken, B., Sexton, G., 1997. Volume loss of the hippocampus and temporal lobe in healthy elderly persons destined to develop dementia. Neurology 48, 1297–1304.

Kemper, T., 1984. Neuroanatomical and neuropathological changes in normal aging and in dementia. In: Albert, M.L., Knopefel, J.E. (Eds.), Clinical Neurology of Aging. Oxford University Press, New York, NY, pp. 9–52.

Killiany, R.J., Gomez-Isla, T., Moss, M., Kikinis, R., Sandor, T., Jolesz, F., Tanzi, R., Jones, K., Hyman, B.T., Albert, M.S., 2000. Use of structural magnetic resonance imaging to predict who will get Alzheimer's disease. Ann. Neurol. 47, 430–439.

Killiany, R.J., Hyman, B.T., Gomez-Isla, T., Moss, M.B., Kikinis, R., Jolesz, F., Tanzi, R., Jones, K., Albert, M.S., 2002. MRI measures of entorhinal cortex vs hippocampus in preclinical AD. Neurology 58, 1188–1196.

Knopman, D.S., Parisi, J.E., Salviati, A., Floriach-Robert, M., Boeve, B.F., Ivnik, R.J., Smith, G.E., Dickson, D.W., Johnson, K.A., Petersen, L.E., McDonald, W.C., Braak, H., Petersen, R.C., 2003. Neuropathology of cognitively normal elderly. J. Neuropathol. Exp. Neurol. 62, 1087–1095.

Kordower, J.H., Chu, Y., Stebbins, G.T., DeKosky, S.T., Cochran, E.J., Bennett, D., Mufson, E.J., 2001. Loss and atrophy of layer II entorhinal cortex neurons in elderly people with mild cognitive impairment. Ann. Neurol. 49, 202–213.

Krimer, L.S., Hyde, T.M., Herman, M.M., Saunders, R.C., 1997. The entorhinal cortex: an examination of cyto- and myeloarchitectonic organization in humans. Cereb. Cortex 7, 722–731.

Langkammer, C., Krebs, N., Goessler, W., Scheurer, E., Yen, K., Fazekas, F., Ropele, S., 2012. Susceptibility induced gray-white matter MRI contrast in the human brain. Neuroimage 59, 1413–1419.

Lee, J., Shmueli, K., Kang, B.T., Yao, B., Fukunaga, M., van Gelderen, P., Palumbo, S., Bosetti, F., Silva, A.C., Duyn, J.H., 2012. The contribution of myelin to magnetic susceptibility-weighted contrasts in high-field MRI of the brain. Neuroimage 59, 3967–3975.

Mesulam, M.M., Mufson, E.J., 1985. The insula of Reil in man and monkey. In: Peters, A., Jones, E.G. (Eds.), Cerebral Cortex, Association and Auditory Cortices. Plenum Press, New York, pp. 179–226.

Meunier, M., Bachevalier, J., Mishkin, M., Murray, E.A., 1993. Effects on visual recognition of combined and separate ablations of the entorhinal and perirhinal cortex in rhesus monkeys. J. Neurosci. 13, 5418–5432.

Meunier, M., Hadfield, W., Bachevalier, J., Murray, E.A., 1996. Effects of rhinal cortex lesions combined with hippocampectomy on visual recognition memory in rhesus monkeys. J. Neurophysiol. 75, 1190–1205.

Mugler III, J.P., Brookeman, J.R., 1991. Rapid three-dimensional T1-weighted MR imaging with the MP-RAGE sequence. J. Magn. Reson. Imaging 1, 561–567.
Murray, E.A., Mishkin, M., 1986. Visual recognition in monkeys following rhinal cortical ablations combined with either amygdalectomy or hippocampectomy. J. Neurosci. 6, 1991–2003.
Murray, E.A., Mishkin, M., 1998. Object recognition and location memory in monkeys with excitotoxic lesions of the amygdala and hippocampus. J. Neurosci. 18, 6568–6582.
Murray, E.A., Bussey, T.J., Hampton, R.R., Saksida, L.M., 2000. The parahippocampal region and object identification. Ann. N. Y. Acad. Sci. 911, 166–174.
Murray, E.A., Graham, K.S., Gaffan, D., 2005. Perirhinal cortex and its neighbours in the medial temporal lobe: contributions to memory and perception. Q. J. Exp. Psychol. B 58, 378–396.
Ono, M., Kubik, S., Abernathey, C.D., 1990. Atlas of the Cerebral Sulci. Georg Thieme Verlag, New York.
Pandya, D.N., Yeterian, E., 1985. Architecture and connections of cortical association areas. In: Peters, A., Jones, E.G. (Eds.), Cerebral Cortex, Association and Auditory Cortices. Plenum Press, New York, pp. 179–226.
Petersen, R.C., Aisen, P.S., Beckett, L.A., Donohue, M.C., Gamst, A.C., Harvey, D.J., Jack Jr., C.R., Jagust, W.J., Shaw, L.M., Toga, A.W., Trojanowski, J.Q., Weiner, M.W., 2010. Alzheimer's Disease Neuroimaging Initiative (ADNI): clinical characterization. Neurology 74, 201–209.
Rosene, D.L., Van Hoesen, G.W., 1987. Cerebral cortex. In: Jones, E.G., Peters, A. (Eds.), Cerebral Cortex, Further Aspects of Cortical Function, Including Hippocampus. Plenum Press, New York, New York.
Sanides, F., 1969. Comparative architectonics of the neocortex of mammals and their evolutionary interpretation. Ann. N. Y. Acad. Sci. 167, 404–423.
Sanides, F., 1970. Functional architecture of motor and sensory cortices in primates in light of a new concept of neocortical evolution. In: Noback, C.R., Montagna, W. (Eds.), The Primate Brain, Advances in Primatology. Appleton-Century Crofts, New York, pp. 137–208.
Segonne, F., Dale, A.M., Busa, E., Glessner, M., Salat, D., Hahn, H.K., Fischl, B., 2004. A hybrid approach to the skull stripping problem in MRI. Neuroimage 22, 1060–1075.
Sigalovsky, I.S., Fischl, B., Melcher, J.R., 2006. Mapping an intrinsic MR property of gray matter in auditory cortex of living humans: a possible marker for primary cortex and hemispheric differences. Neuroimage 32, 1524–1537.
Solodkin, A., Van Hoesen, G.W., 1996. Entorhinal cortex modules of the human brain. J. Comp. Neurol. 365, 610–617.
Stephan, H., 1975. In Handbuch der mikroskopischen Anatomie des Menschen. Springer-Verlag, Berlin and New York.
Suzuki, W.A., Amaral, D.G., 1994a. Perirhinal and parahippocampal cortices of the macaque monkey: cortical afferents. J. Comp. Neurol. 350, 497–533.
Suzuki, W.A., Amaral, D.G., 1994b. Topographic organization of the reciprocal connections between the monkey entorhinal cortex and the perirhinal and parahippocampal cortices. J. Neurosci. 14, 1856–1877.
Suzuki, W.A., Amaral, D.G., 2003a. Perirhinal and parahippocampal cortices of the macaque monkey: cytoarchitectonic and chemoarchitectonic organization. J. Comp. Neurol. 463, 67–91.
Suzuki, W.A., Amaral, D.G., 2003b. Where are the perirhinal and parahippocampal cortices? A historical overview of the nomenclature and boundaries applied to the primate medial temporal lobe. Neuroscience 120, 893–906.
Suzuki, W.A., Zola-Morgan, S., Squire, L.R., Amaral, D.G., 1993. Lesions of the perirhinal and parahippocampal cortices in the monkey produce long-lasting memory impairment in the visual and tactual modalities. J. Neurosci. 13, 2430–2451.
Taylor, K.I., Probst, A., 2008. Anatomic localization of the transentorhinal region of the perirhinal cortex. Neurobiol. Aging 29, 1591–1596.
van Gelderen, P., de Zwart, J.A., Lee, J., Sati, P., Reich, D.S., Duyn, J.H., 2012. Nonexponential T(2) decay in white matter. Magn. Reson. Med. 67, 110–117.
Van Hoesen, G.W., 1995. Anatomy of the medial temporal lobe. Magn. Reson. Imaging 13, 1047–1055.
Van Hoesen, G., Pandya, D.N., 1975a. Some connections of the entorhinal (area 28) and perirhinal (area 35) cortices of the rhesus monkey. I. Temporal lobe afferents. Brain Res. 95, 1–24.
Van Hoesen, G.W., Pandya, D.N., 1975b. Some connections of the entorhinal (area 28) and perirhinal (area 35) cortices of the rhesus monkey. III. Efferent connections. Brain Res. 95, 39–59.
Van Hoesen, G.W., Solodkin, A., 1993. Some modular features of temporal cortex in humans as revealed by pathological changes in Alzheimer's disease. Cereb. Cortex 3, 465–475.
Van Hoesen, G.W., Augustinack, J.C., Dierking, J., Redman, S.J., Thangavel, R., 2000. The parahippocampal gyrus in Alzheimer's disease. Clinical and preclinical neuroanatomical correlates. Ann. N. Y. Acad. Sci. 911, 254–274.
von Economo, C.F., Koskinas, G.N., 1925. Die Cytoarchitektonik der Hirnrinde des erwachsenen Menschen (Cytoarchitectonics of the Adult Human Cerebral Cortex). Springer, Berlin.
Xu, Y., Jack Jr., C.R., O'Brien, P.C., Kokmen, E., Smith, G.E., Ivnik, R.J., Boeve, B.F., Tangalos, R.G., Petersen, R.C., 2000. Usefulness of MRI measures of entorhinal cortex versus hippocampus in AD. Neurology 54, 1760–1767.
Zhan, J., Brys, M., Glodzik, L., Tsui, W., Javier, E., Wegiel, J., Kuchna, I., Pirraglia, E., Li, Y., Mosconi, L., Saint Louis, L.A., Switalski, R., De Santi, S., Kim, B.C., Wisniewski, T., Reisberg, B., Bobinski, M., de Leon, M.J., 2009. An entorhinal cortex sulcal pattern is associated with Alzheimer's disease. Hum. Brain Mapp. 30, 874–882.
Zola-Morgan, S., Squire, L.R., Amaral, D.G., Suzuki, W.A., 1989. Lesions of perirhinal and parahippocampal cortex that spare the amygdala and hippocampal formation produce severe memory impairment. J. Neurosci. 9, 4355–4370.